Article

Covalent Grafting of Eosin Y to the Giant Keplerate {Mo$_{132}$} through an Organosilicon Linker in Homogeneous Regime

Andrey Denikaev [1], Grigory Kim [1,2], Evgeny Greshnyakov [1], Nikolai Moskalenko [3] and Kirill Grzhegorzhevskii [1,2,*]

[1] Institute of Natural Sciences and Mathematics, Ural Federal University, Mira St. 19, Ekaterinburg 620002, Russia; andrejdenikaev@gmail.com (A.D.); kim-g@ios.uran.ru (G.K.); evgeny.greshnyakov@urfu.ru (E.G.)

[2] I. Ya. Postovsky Institute of Organic Synthesis of the Ural Branch of RAS, 22/20 S. Kovalevskoy/Akademicheskaya St., Ekaterinburg 620108, Russia

[3] Institute of High Temperature Electrochemistry of the Ural Branch of RAS, 22 S. Kovalevskoy St./20 Akademicheskaya St., Ekaterinburg 620066, Russia; moskalenko.nikol@yandex.ru

* Correspondence: kirillvalentinovich@urfu.ru

Abstract: The template effect of giant polyoxometalates (POM) shows promising results towards the supramolecular design of hybrid materials suitable for photocatalytic reactions. Here, we demonstrate a novel synthetic approach for covalently grafting the xanthene dye eosin Y (EY) to the nanoscale Keplerate POM {Mo$_{132}$} via an organosilicon linker (3-aminopropyltrimethoxysilane, APTMS) in a homogeneous regime. Using a phase transfer agent, tetrabutylammonium bromide, we solubilize the Keplerate POM modified with six {Si(CH$_2$)$_3$NH$_2$} groups, {Mo$_{132}$}@Si$_6$, in a series of organic solvents—acetonitrile, acetone, tetrahydrofuran, and dichloromethane—to perform post-functionalization by using an NHS-ester of EY. Both IR and Raman spectroscopy affirm the preservation of the POM's structure and showcase an amide bond formation between POM and EY in the obtained conjugate {Mo$_{132}$}@Si$_6$@EY@TBA. Grafting's success is observed through significant downfield shifting of EY's aromatic protons' signals on the ^{1}H NMR spectrum as compared to the spectra of EY and EY-NHS. The current synthetic approach enables us to exercise precise control of the stoichiometry in the POM-dye conjugates—1:1 for the POM-EY system—as confirmed by elemental analysis. Comprehensive photophysical analysis of {Mo$_{132}$}@Si$_6$@EY@TBA by means of UV-Vis and steady-state and time-resolved fluorescence measurements points to an existing strong interaction between molecular orbitals of EY and {Mo$_{132}$}, leading to a photoinduced electron transfer, partial fluorescence quenching, and elongation of the excited state's lifetime. These findings demonstrate that using APTMS as an organosilicon linker in tandem with the Keplerate POM as a nanoscale template can be readily applied as a routine synthetic procedure for grafting various organic dyes or other organic molecules bearing a carboxylic group in their structure to the giant POM surface in a variety of aprotic organic solvents.

Keywords: conjugation; polyoxometalates; eosin Y; Keplerate; electron transfer; fluorescence; photocatalysis; supramolecular structure

1. Introduction

Supramolecular design of photocatalytic nanoscale units, such as nano-reactors or bulk materials based on polyoxometalates (POM), is a challenging task. Despite the fact that combining different inorganic clusters and organic sensitizers gives plenty of variation for finding the desired photophysical properties, the specifics of how conjugation between inorganic and organic components occurs have not been thoroughly investigated. Both electrostatic interactions and covalent grafting are suitable for the synthesis of hybrid supramolecular structures. However, both approaches have significant limitations. Electrostatic interactions occur only between oppositely charged species and, most often,

require aqueous media in which they can take place. Such molecular associations are well known for giant POMs (namely, toroidal type {Mo_{138}} and Keplerate type {Mo_{132}}) and cationic dyes of different natures: xanthene dye rhodamine B [1,2] and porphyrin dye H_2TMPyP [3]. An association between cationic porphyrin and simple polyoxoanions, such as Keggin [$SiW_{12}O_{40}$]$^{4-}$ or lacunary Wells–Dawson, can also be produced [4]. Namely, the layer-by-layer technique is used for the fabrication of electrodes for oxygen reduction reactions based on [$\alpha_2Fe^{III}P_2W_{17}O_{61}$]$^{7-}$ and tetracationic porphyrin [5]. Interestingly, in electrostatic associates, due to the photoinduced electron transfer (PET), effective charge separation often occurs in an excited state, leading to complete fluorescence quenching.

Unlike linking through electrostatics, covalent grafting requires a more complex and detailed synthetic approach, but one can surpass the limitations caused by the dye and solvent nature. Hydrophobic BODIPY derivatives can be grafted to the Keggin POM through organosilicon and organotin linkers, leading to rapid photoinduced charge separation [6]. When the Ir-based sensitizer is conjugated with Anderson-type polyoxomolybdate, the charge transfer process becomes incredibly sensitive to the nature of the molecular linkers used [7,8]. Thus, the nature of the molecular linker between inorganic and organic components plays a vital role in successful grafting. In addition to the linker's nature, the type of counterions and the solvent's dipole moment affect the PET process in the dye-POM conjugates. For instance, for the BODIPY-lacunary Dawson α_2-[$P_2W_{17}O_{61}$]$^{10-}$ conjugate anchored by the Si-O-Si group, the time of photoinduced charge separation (CS) decreases from 380 ps to 82 ps when counterions vary from bulkier tetrabutylammonium to smaller tetramethylammonium. The trend holds when the solvent's polarity is being increased [9]. J. Poblet, E. Gibson, and G. Izzet report that CS between organic dyes and POMs occurs through the space within the Marcus normal region [9]. This electron transfer mechanism is demonstrated in the dye-sensitized solar cell comprising the nanostructured mesoporous ITO film with grafted push–pull luminophore [10], where the introduction of tin-substituted lacunary Keggin [$PW_{11}O_{39}SnR$]$^{3-}$ enhances the cell's photoefficiency. Aside from providing precise control of the charge separation efficiency, the electropolymerization of both Keggin- and Dawson-type POMs, bearing two remote pyridyl groups, with porphyrin dyes also allows for the production of copolymer films with photocurrent generation capabilities [11]. Furthermore, photo-switchable molecules, such as spiropyran [12] and benzospiropyran [13], when grafted to Anderson- and Keggin-type POMs, experience a significant increase in the fluorescence quantum yield due to the extra population of their excited state as compared to the individual luminophore molecules.

In contrast with the grafting of different dyes to simple POMs (Anderson–Evans, Keggin, Wells–Dawson, etc.) [14–17], the use of giant POM structures is still in its early stages. If one breaks through this task, the giant POM can serve as a nanoscale template for the step-by-step design of desired supramolecular ensembles on its surface. We believe that this concept, which allows for a combination of sensitizer, chiral inductor, guest pore, and other suitable scaffolds, is capable of reaching optimally tuned smart photocatalytic systems. In addition to their template effect, the giant POMs exhibit dynamic self-assembling behavior and, thus, can form hollow blackberry-type vesicles [18,19]. This process is controlled through the fine tune of POM's surface charge density [20–23]. Therefore, due to covalent grafting, one can combine both functionalization strategy and dynamic organization to develop novel hierarchical nanomaterials as it is well known for simple POMs [24–26].

However, despite the appeal of using giant POMs for conjugation with different organic molecules, the choice of an appropriate linker remains crucial. By using 3-aminopropyltrimethoxysilane (APTMS), we terminate Keplerate {Mo_{132}}'s surface with a desired number of amino groups (up to 60), allowing for easy post-modification via an amide bond formation [27,28]. The modification of {Mo_{132}} with APTMS leads to a dropdown in solubility of the conjugate {Mo_{132}}@Si_{60}. However, for species with 20 or fewer ({Mo_{132}}@Si_{20}) structural elements, both the degree of modification and solubility remain at appropriate levels for post-functionalization. Following this synthetic approach, we covalently graft an anionic dye—fluorescein (FL)—to the {Mo_{132}}@Si_{18} cluster. As a

result, a novel charge transfer band at 529–532 nm appears on the UV-Vis spectrum, corresponding to the PET from the HOMO state of the POM to the LUMO state of fluorescein. This is opposite from the direction of the PET process in the electrostatic associates between $\{Mo_{132}\}$ and cationic dyes [2,3]. Therefore, covalent grafting paves the way to control the charge transfer within the giant POM-based supramolecular structures.

Despite the success of the fluorescein grafting to the $\{Mo_{132}\}$, the structural composition of these conjugates is still difficult to control as the reaction between fluorescein-NHS and $\{Mo_{132}\}@Si_{18}$ occurs in a non-homogeneous regime. In addition, it is difficult to purify the $\{Mo_{132}\}@Si_{18}@FL_x$ conjugates from residual unbounded dye due to the limited solubility of the fluorescein dye using common organic solvents. Thus, we cannot elucidate what exact influence the conjugation between the dye and the giant POM has on the dye's photophysical properties without the contribution of other side processes that arise from dye-to-dye interactions on the POM's surface.

To resolve the aforementioned issues posed by the described approach, we suggest an improved synthetic route that allows for covalent grafting of different organic dyes, bearing at least one carboxylic group, to the $\{Mo_{132}\}$ with the desired stoichiometry of POM:dye = 1:1 in a homogeneous regime and in a variety of aprotic organic solvents (acetonitrile, acetone, tetrahydrofuran, and dichloromethane). Using the APTMS-linker, we produced the $\{Mo_{132}\}@Si_6$ POM, which was transferred to the organic phase with tetrabutylammonium (TBA) cations and modified with eosin Y (EY) NHS-ester (EY-NHS). Obtained conjugate, $\{Mo_{132}\}@Si_6@EY@TBA$, was investigated with IR and Raman spectroscopy to affirm the integrity of the Keplerate structure and ensure complete conversion of the EY-NHS to the final product. ^{1}H NMR spectra showcased significant downfield shifts of the aromatic signals from EY molecules when grafted to the POM's surface. The stoichiometry between POM and dye in the $\{Mo_{132}\}@Si_6@EY@TBA$ was evaluated through elemental analysis (C, N, H, Mo, and Si). Comprehensive analysis of the photophysical parameters—UV-Vis, as well as steady-state and time-resolved fluorescence measurements—revealed the strong interaction between molecular orbitals of the EY and $\{Mo_{132}\}$. The obtained results demonstrated the significant potential of the suggested approach for the fabrication of novel photocatalytic systems using the giant POM as a nanoscale template.

2. Results and Discussion

2.1. Conjugation of Esoin Y with {Mo132}

The conjugation procedure of the giant POM $\{Mo_{132}\}$ consists of several stages (Figure 1). First, the Keplerate should be functionalized with amino groups. As we recently showed, it can be effectively performed by using APTMS molecules as an organosilicon linker in methanol under an argon atmosphere [28]. Because APTMS exclusively reacts with dimolybdenum units, $\{Mo_2\}$ (30 $\{Mo_2\}$ per $\{Mo_{132}\}$), the modification degree of POM can be controlled by defining a molar ratio between the organosilicon linker and the Keplerate in solution. Though linking six $\{Si(CH_2)_3NH_2\}$ groups to the POM's surface does not decrease the solubility of the produced $\{Mo_{132}\}@Si_6$ complex in methanol, this solvent is not appropriate for any further reaction with the NHS-ester. For such a reaction, we would be expected to use acetonitrile, in which $\{Mo_{132}\}@Si_6$ is poorly soluble. Indeed, the amide bond formation between the NH_2 group and an activated carbon atom in the NHS-ester is much more effective when it occurs in a homogeneous regime of aprotic solvents and an added base. Therefore, we lyophilize the $\{Mo_{132}\}@Si_6$ by its extraction from an aqueous phase to chloroform with a 504-fold molar excess of TBAB. Due to the cationic exchange between NH_4^+ and TBA, the $\{Mo_{132}\}@Si_6@504TBA$ salt is obtained. Lastly, we perform the target reaction in a variety of aprotic organic solvents, such as acetonitrile, acetone, tetrahydrofuran (THF), and dichloromethane (DCM), with the EY-NHS ester to synthesize the $\{Mo_{132}\}@Si_6@EY@TBA$ conjugate.
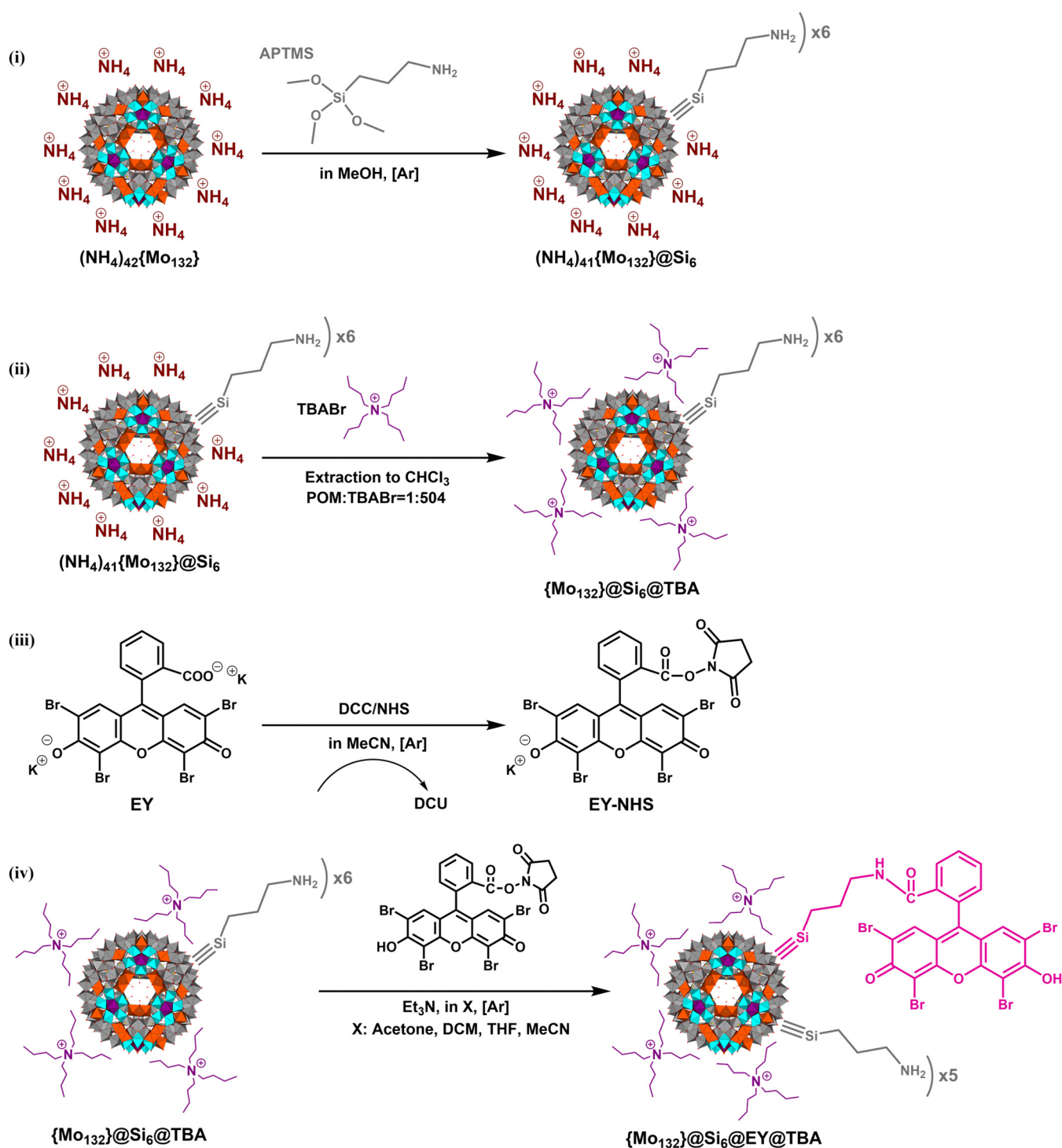
Figure 1. Schematic of $\{Mo_{132}\}$ modification with EY dye via APTMS linker: (**i**) grafting of six $\{Si(CH_2)_3NH_2\}$ groups to the POM's surface; (**ii**) transfer of the $\{Mo_{132}\}@Si_6$ to chloroform by adding 504-fold molar excess of TBAB; (**iii**) synthesis of NHS-ester of EY; and (**iv**) grafting of EY dye to the $\{Mo_{132}\}@Si_6@TBA$ through an amide bond in aprotic organic solvents.

The IR spectrum of the $\{Mo_{132}\}@Si_6@EY@TBA$ conjugate, produced in acetonitrile, shows an amide I band at 1670 cm^{-1} and simultaneous diminishing of the carbonyl stretching at 1774 and 1739 cm^{-1} of EY-NHS [29], demonstrating that the EY grafting to the NH$_2$ groups has occurred (Figures 2 and S1, see Supporting Information). An intense band at 2114 cm^{-1}, corresponding to a strongly H-bonded hydroxyl group or

dimers in EY-NHS, also disappears upon conjugation with $\{Mo_{132}\}@Si_6@504TBA$. The presence of the $\{Si(CH_2)_3NH_2\}$ groups is affirmed by observing a weak stretching from the propylsilane structure at 1226 cm^{-1}. Namely, for $\{Mo_{132}\}@Si_{18}$, this stretching appears at around 1225 cm^{-1} [28] due to the formation of the siloxane bonds between grafted APTMS linkers. Compared to $\{Mo_{132}\}$, we observe numerous other spectral features from the $\{Mo_{132}\}@Si_6@EY@TBA$ that have to do with the exchange between the NH_4^+ cations and TBA molecules. To illustrate these features, we compare the IR spectra of $\{Mo_{132}\}$ and the TBA salt of $\{Mo_{132}\}@Si_6$. The cationic exchange is clearly observed through the substitution of the $\nu(NH_4^+)$ band at 1410 cm^{-1} by the band at 1474 cm^{-1} from TBA. Other TBA-related bands appear without any shifting on the spectrum of the $\{Mo_{132}\}@Si_6@504TBA$ except one sharp intense band at 1260 cm^{-1} which relates to aliphatic chains' stretching in ordered state. In the fingerprint region sensitive to the Keplerate's vibrations, two stretching bands of terminal oxo groups, namely $\nu(O-Mo-O)$ and $\nu(Mo=O)$ [30], at 970 cm^{-1} and 937 cm^{-1}, become sharper and shift further to 979 cm^{-1} and 947 cm^{-1}, respectively. High-frequency shifts of these bands correspond to an increase in the bond force constant (or bond order) in the terminal $Mo=O/Mo-O$ groups as TBA does not participate in hydrogen bonding with the oxo groups, unlike NH_4^+ cations. Furthermore, the exchange between the NH_4^+ cations and TBA should result in an increase in the reduced mass value, leading to a low-frequency shift of the aforementioned stretching bands. Therefore, the breaking of the hydrogen bonds dominates the expected changes in the reduced mass and causes a high-frequency shift that is observed for the $Mo=O/Mo-O$ groups. Interestingly, for the $\{Mo_{132}\}@Si_6@TBA$, an entirely novel shoulder at 708 cm^{-1} appears. This band is located near the stretching frequency of the bridging bonds—$Mo-\mu_2O-Mo/Mo-\mu_3O-Mo$—at 729 cm^{-1} [30].
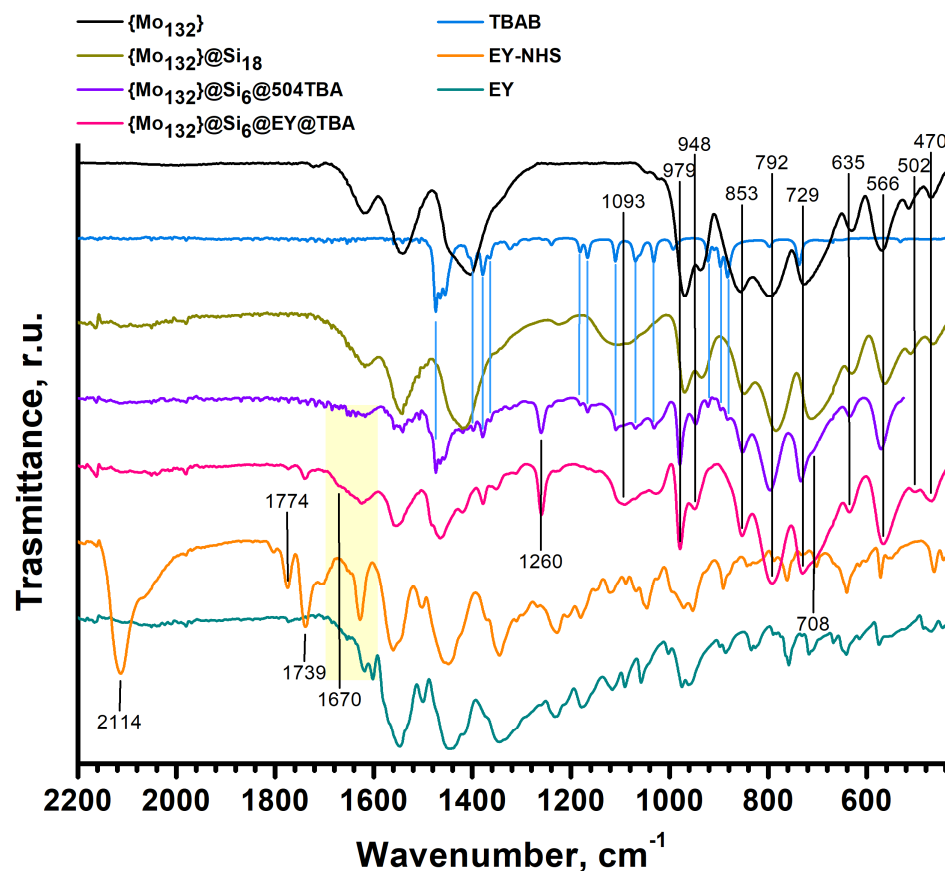

Figure 2. IR spectra measured at ATR mode of the (from bottom to top): EY, EY-NHS, $\{Mo_{132}\}@Si_6@EY@TBA$, $\{Mo_{132}\}@Si_6@504TBA$, $\{Mo_{132}\}@Si_{18}$, TBAB, and $\{Mo_{132}\}$.

Taking into account that the negative charge of the {Mo_{132}} is mostly localized in dimolybdenum structural units [31] containing the Mo-μ_2O-Mo bridges, the interaction between the {Mo_2} and the TBA likely brings nonequivalence to the bridging bonds' stretching.

Raman spectroscopy allows for monitoring the preservation of the Keplerate structure's integrity upon grafting of EY to the {Mo_{132}}@Si_6@504TBA (Figure 3). The observation of A_g and H_g totally symmetric modes reaffirms the presence of {Mo_{132}} in the {Mo_{132}}@Si_6@EY@TBA conjugate. The A_g band (the breathing vibration of the terminal oxo groups) undergoes a high-frequency shift from 876 cm^{-1} to 882 cm^{-1}, similar to the band at 944 cm^{-1} (the stretching of the Mo=O in substructural units) that is shifting to 973 cm^{-1}. This trend is consistent with the IR data of the terminal oxo groups. In contrast, both the H_g (the breathing stretching of the Mo-O-Mo bonds) and the bending vibration δ (Mo=O) of the substructural units exhibit a small low-frequency shift from 376 cm^{-1} and 314 cm^{-1} to 375 cm^{-1} and 310 cm^{-1}, respectively. The observed low-frequency shifts are likely due to an increase in reduced mass for the {Mo_{132}}@Si_6@TBA as compared to pure {Mo_{132}} [30]. The presence of EY's xanthene core can be evaluated through the appearance of aromatic bands at 1503 cm^{-1} and 1633 cm^{-1}. The EY-NHS formation slightly changes these bands' positions to 1507 cm^{-1} and 1628 cm^{-1}, respectively. Further grafting of EY to the POM results in the shifting of these bands to 1522 cm^{-1} and 1629 cm^{-1}. Such significant shifts (from 1503 cm^{-1} in the free dye form to 1522 cm^{-1} in the conjugate) are related to the electron density rearrangement within the xanthene core [32] upon conjugation with {Mo_{132}}. It is worth noting that the Raman spectra of EY and EY-NHS indicate strong contributions from the dye's fluorescence signal. Conjugation with POM leads to an improved signal-to-noise ratio due to a partial fluorescence quenching of EY.
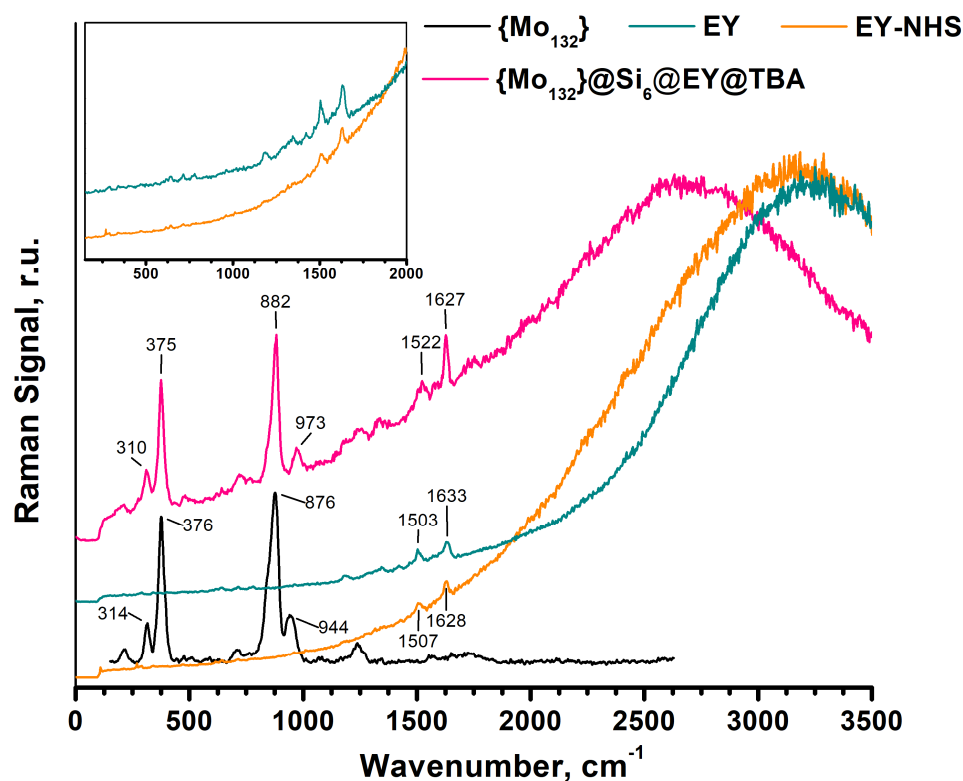

Figure 3. Raman spectra of {Mo_{132}} (measured with 633 nm He-Ne laser), EY, EY-NHS, and {Mo_{132}}@Si_6@EY@TBA (measured with 488 nm laser). All measured samples were used in powder form. Insert shows magnified spectra of EY and EY-NHS, where the xanthene core signals are observed.

The most substantial evidence of successful EY grafting to the $\{Mo_{132}\}@Si_6$ can be inferred from the ^{1}H NMR spectra of the $\{Mo_{132}\}@Si_6@EY@TBA$. The full-range proton NMR spectra for EY, EY-NHS, and $\{Mo_{132}\}@Si_6@EY@TBA$ are presented in Figures S2–S4 (see Supporting Information) and analyzed in detail in the experimental section. As EY is being grafted via an amide bond, the carboxyphenyl protons should exhibit high sensitivity towards conversion of the COOH group to the NHS-ester and to the C(O)-NH- amide group. These changes are illustrated in Figure 4. In aprotic solvents, such as MeCN, EY can exist in two forms: open and closed (spiro or lactonic form) [33]. This results in signals splitting, with more deshielded signals coming from the open form. Namely, f and f'-protons appear at 8.10 ppm and 8.07 ppm, respectively. Integrating these signals, we calculate the ratio between the open and closed forms to be 2:1 (Figure S2, see Supporting Information). The conversion of EY to the EY-NHS ester leads to an intensified electron-withdrawing effect from the phenyl group and causes the deshielding of the *f* proton to 8.31 ppm. The EY-NHS ester cannot exist in the lactonic form, which is also consistent with the NMR data. It is important to note that, during the EY-NHS preparation, there remains some residual amount of the reaction's side product—dicyclohexylurea (DCU)—forming an intermolecular complex with the EY-NHS, which is stabilized by hydrogen bonding. This does not affect the reactivity of the EY-NHS for the target reaction but does complicate the NMR spectrum interpretation (Figure S3, see Supporting Information). Upon conjugation of the $\{Mo_{132}\}@Si_6@504TBA$, the open-closed form equilibria are established as suggested by the signal splitting: f and f' protons at 8.35 ppm and 8.32 ppm, respectively. Both doublets (f and f') are shifted by 0.25 ppm as compared to the free EY molecule. Other aromatic protons from the phenyl group are deshielded too. For instance, d' protons undergo a downfield shift from 7.54 ppm (in EY) to 7.97 ppm (upon conjugation with POM) (Figure S4, see Supporting Information). Interestingly, the ratio between the open and the closed form of the EY molecules that are grafted to POM is calculated to be 1:1. Further analysis of the aromatic protons suggests that some residual amounts of chloroform and toluene molecules are still present in the $\{Mo_{132}\}@Si_6@EY@TBA$ sample (from washing procedure), remaining encapsulated within the Keplerate's cavity due to a slow exchange between water and methanol or toluene. The latter undergoes partial exchange with chloroform during the last synthetic step (Figure 1).

The TBA cations exhibit four well-known signals: three methylene groups at the α (3.28 ppm), β (1.75 ppm), and γ (1.49 ppm) positions and one methyl group at the δ position (1.01 ppm) (Figure S4, see Supporting Information).

Integrating the TBA proton signals, we observe the ratio between EY (both open and closed form) and TBA to be 1:31. The signals from the APTMS linker overlap with different alkyl radicals and cannot be observed directly on the NMR spectrum. Even for the $\{Mo_{132}\}@Si_6$ species, the APTMS signals are absent on the ^{1}H NMR spectrum in D_2O (data are not presented here). One possible reason for that is the decrease in protons' mobility for organic molecules located on the Keplerate's surface as it has been observed for the $\{Mo_{132}\}@Porphyrin$ associates [3]. For instance, the POM's effect on the NMR signal from the acetate groups located in the inner cavity of the Keplerate structure is well studied and is observed as a wide band near 0.7 ppm. Without the POM-induced shielding effect, the signal from free acetate molecules appears near 2 ppm [34].
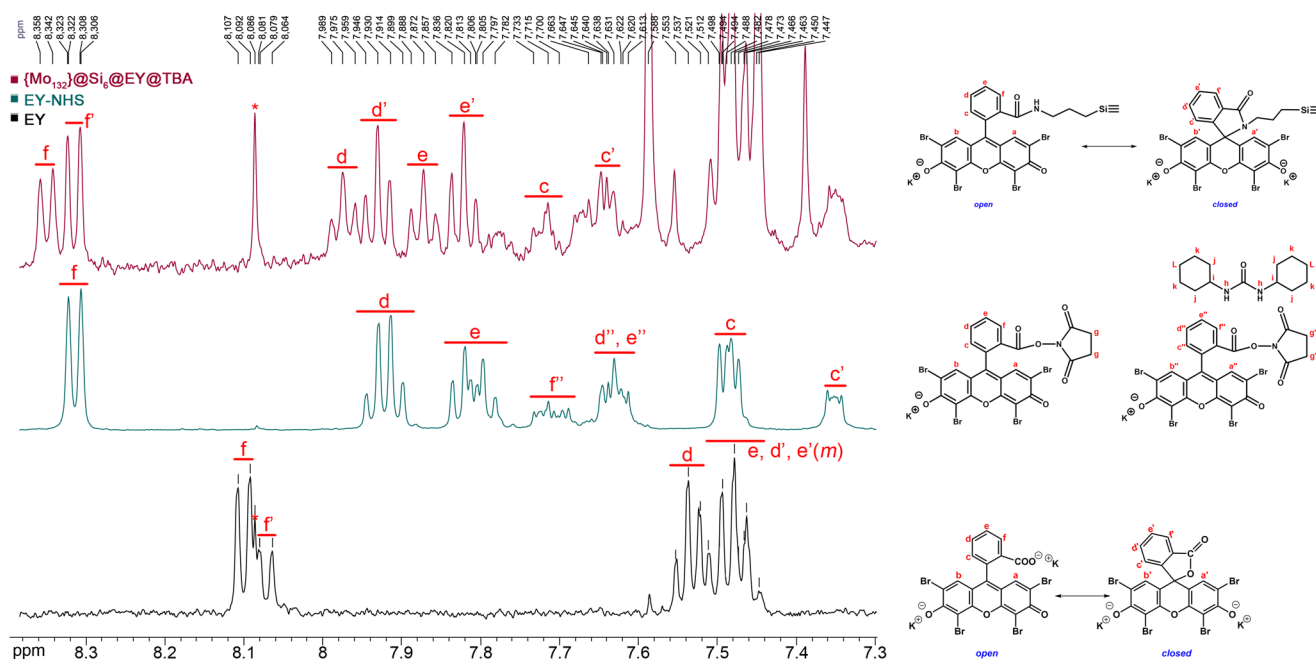
Figure 4. ^{1}H NMR spectra (in CD_3CN) of EY, EY-NHS, and $\{Mo_{132}\}@Si_6@EY@TBA$ (from bottom to top). Signal marked with (*) is impurity. For signals attribution (a, a', a'' etc.) see the Experimental section.

To elucidate the structural composition of the $\{Mo_{132}\}@Si_6@EY@TBA$, elemental analysis was performed. After the first modification step, elemental analysis for the $\{Mo_{132}\}@Si_6$ shows the Mo:Si ratio to be 132:6 and CNH content to be 4.85%, 2.64%, and 2.35%. The proposed formula for the $\{Mo_{132}\}@Si_6$ complex is $(NH_4)_{41}[Mo^{VI}_{72}O_{252}Mo^V_{60}O_{120}(SiCH_2CH_2CH_2NH_2)_6(CH_3COO)_{29}(H_2O)_{72}]\cdot 4CH_3OH\cdot 3C_6H_5CH_3\cdot 51H_2O$. For the conjugate $\{Mo_{132}\}@Si_6@EY@TBA$, the CNH content is as follows: 29.32%, 1.69%, and 6.29%. Considering the EY:TBA and chloroform:toluene ratios determined from the NMR spectrum, the proposed formula for the conjugate is $TBA_{31}[Mo^{VI}_{72}O_{252}Mo^V_{60}O_{120}(SiCH_2CH_2CH_2NH_2)_5(SiCH_2CH_2CH_2NH)(CH_3COO_{29})(H_2O)_{72}\{C_{20}H_6Br_4O_4\}]\cdot 35C_6H_5CH_3\cdot 5CHCl_3\cdot 5CH_3CN\cdot 214H_2O = \{Mo_{132}\}@Si_6@EY@TBA$. The presence of H_2O molecules in the outer sphere of the POM is due to the washing from the unreacted EY-NHS molecules with water (Figure 1).

2.2. Analysis of Photophysical Properties of $\{Mo_{132}\}@Si_6@EY@TBA$

Conjugation of EY with $\{Mo_{132}\}@Si_6$ can be observed on the UV-Vis (Figure 5) and fluorescence spectra (Figure 6). Due to the washing procedure aimed at the removal of the unreacted EY in chloroform, UV-Vis spectra for individual components and for the conjugate are collected and analyzed only in $CHCl_3$ even though the synthesis of $\{Mo_{132}\}@Si_6@EY@TBA$ is performed in another aprotic solvent (MeCN, acetone, THF, and DCM), (Figure 5a). For EY, EY-NHS, and $\{Mo_{132}\}@Si_6@EY@TBA$, the dye's band characteristic of the HOMO-LUMO transition is shifted from 529 nm to 543 nm. Interestingly, for the EY solution, containing TBABr of the same concentration as in the case of $\{Mo_{132}\}@Si_6@504TBA$ synthesis, the HOMO-LUMO band of EY does not undergo any redshifting and appears at 528 nm. Along with EY, the LMCT band of $\{Mo_{132}\}$ is also shifted to longer wavelengths: from 455 nm to 477 nm. This shift is induced by the formation of the TBA salt of POM as suggested by the UV-Vis spectra of the reference sample $\{Mo_{132}\}@504TBA$ measured in different organic solvents (Figure S5a, see Supporting Information).
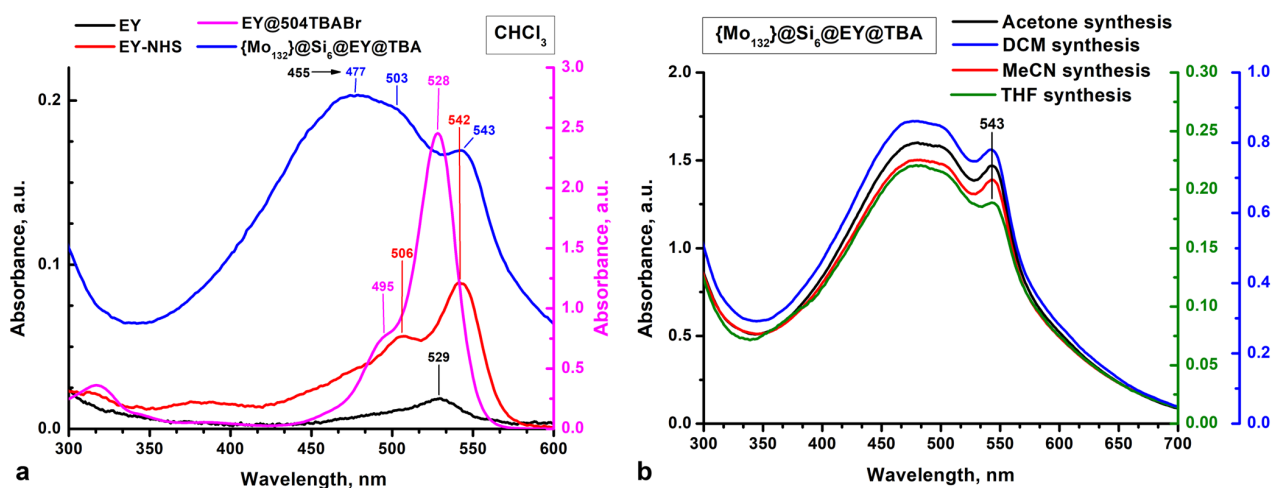
Figure 5. (**a**) UV-Vis spectra of {Mo$_{132}$}@Si$_6$@EY@TBA, {Mo$_{132}$}@Si$_6$@504TBA, EY-NHS, and EY in chloroform; (**b**) in chloroform, UV-Vis spectra of {Mo$_{132}$}@Si$_6$@EY@TBA synthesized in different organics solvents.
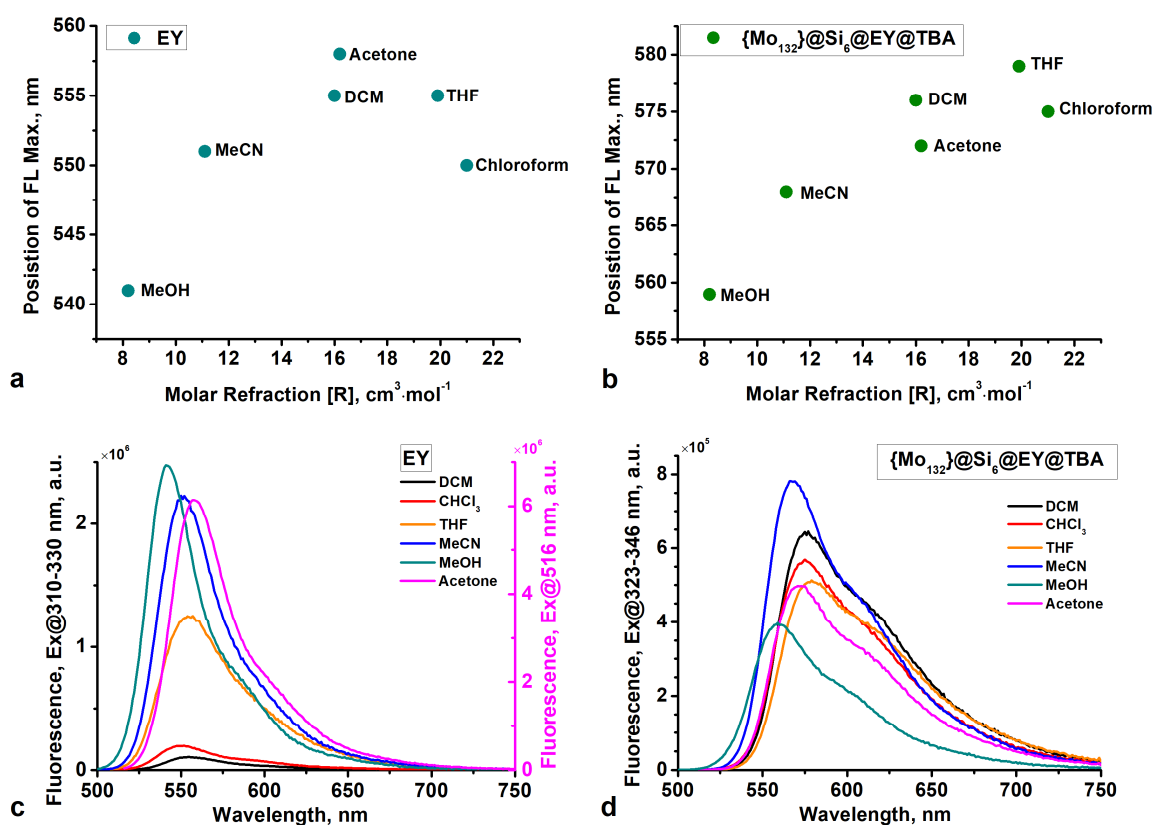

Figure 6. (**a**,**b**) Main fluorescence signal's position against molar refraction (R) for a series of organic solvents for EY and {Mo$_{132}$}@Si$_6$@EY@TBA; (**c**,**d**) Steady-state fluorescence spectra of EY and {Mo$_{132}$}@Si$_6$@EY@TBA in a series of organic solvents. Except for the EY solution in DCM and chloroform, in which the dye is poorly soluble, the concentration of the sample remained constant across all examined solutions.

To reveal the effect of the conjugation process with POM on the EY, we compare the absorbance of EY, {Mo$_{132}$}@504TBA, and their mixture at molar ratio EY:POM = 1:1 on the UV-Vis spectrum (Figure S5, see Supporting Information). On the UV-Vis spectrum of EY, we observe solvatochromism as indicated by the HOMO-LUMO band shifting from

522 nm (in MeOH) to 539 nm (in acetone). In addition, it is worth noting that the solvent's nature affects the oscillator strength of the HOMO-LUMO transition in the EY molecule. Namely, dissolving EY in THF reduces the absorbance intensity at 530 nm practically two times as compared to the acetone solution with the same dye concentration, as shown in Figure S5d (see Supporting Information). Considering the aforementioned features of EY, we can compare the UV-Vis spectra of the conjugate $\{Mo_{132}\}@Si_6@EY@TBA$ and a stoichiometrically equivalent mixture of EY and $\{Mo_{132}\}@504TBA$ (Figures 5b and S5b; see Supporting Information).

For this mixture of EY and $\{Mo_{132}\}@504TBA$, the dye's HOMO-LUMO band demonstrates solvatochromism (maximum's position at 514 nm and at 531 nm for MeOH and acetone, respectively) and appears as a weak shoulder on the POM LMCT band (Figure S5b; see Supporting Information). In contrast, in the case of the $\{Mo_{132}\}@Si_6@EY@TBA$, the dye's HOMO-LUMO transition is observed as a strong band at 543 nm as compared to 529 nm for EY in chloroform. We assume that this absorbance maximum experiences a strong contribution from a novel charge-transfer band. This transition should correspond to the PET process between some molecular orbitals separated by a distance of 2.3 eV. For pure Keplerate $\{Mo_{132}\}$, the HOMO level is located at −5.8 eV [35] and at −5.25 eV for EY [36]. The LUMO level of pure EY is approximately at −3.05 eV (in accordance with the Tauc plot), but upon grafting to POM via an amide bond, this level can be shifted, resulting in the PET from the ground state of $\{Mo_{132}\}$ to the LUMO of EY.

The steady-state fluorescence measurements of EY also show solvatochromism in a series of organic solvents: methanol, acetonitrile, DCM, acetone, THF, and chloroform (Figure 6). For all solvents, the fluorescence signal of EY consists of the main component (band no. 1) and a shoulder (band no. 2) on its right side. In accordance with Kasha's rule, the fluorescence transition occurs from the LUMO state. Therefore, these two components within one signal correspond to different molecular species. One of them is EY (band no. 1), wherein another one likely belongs to the dimeric form of EY (such as J-aggregates) [37]. Additionally, the interaction between the open and closed forms of EY can contribute to the appearance of band no. 2.

The spectral shift of band no. 1 correlates well with the molar refraction (R) of the corresponding solvents (Figure 6a). The observed dependency has a bell-like shape for EY due to the specific solvation effect, most notably in acetone, THF, and chloroform. The stronger the interaction between the solvent molecules and EY in its excited state, the greater the observed redshifts of the fluorescence band [38]. Consequently, the decrease in the redshift of EY in chloroform can be attributed to the poor solubility of the dye molecules in this solvent due to certain thermodynamic factors. After conjugation with $\{Mo_{132}\}@Si_6$, the dependency of the fluorescence maxima on the molar refraction is linear (Figure 6b). As the $\{Mo_{132}\}@Si_6@EY@TBA$ conjugate is highly soluble in all examined solvents, the data from chloroform are fitted better by a common linear trend. However, for both acetone and chloroform—solvents with the highest and the lowest solubility of EY, respectively—the data slightly deviate from the linear fit compared to other solvents.

This points to some specific interactions between these solvents' molecules and the EY molecules in their ground and/or excited states. Interestingly, upon conjugation with POM, the fluorescence intensity of EY drops down by an order of magnitude (Figure 6d), and the contribution from band no. 2 increases. In line with such behavior, the open-to-closed form ratio changes from 2:1 for EY to 1:1 for $\{Mo_{132}\}@Si_6@EY@TBA$. This indirectly points to the contribution from the open-closed form equilibrium to the presence of band no. 2.

Fluorescence excitation spectra show an apparent decrease in intensity of the band at 500 nm, while the band near 530 nm increases in intensity and shifts to the long-wavelength region upon conjugation with POM (Figure S6, see Supporting Information). Namely, the distance between band no. 1 and its corresponding maximum on the fluorescence excitation spectrum jumps from 20 nm to 25 nm upon conjugation of EY with POM. These results are also consistent with the appearance of the charge-transfer band at 543 nm on the UV-Vis spectra (Figure 5b). The influence of conjugation between EY and POM on the fluorescence

properties can be evaluated by measuring the quantum yield (Φ_F) and the lifetime of the excited state (τ) (Figures S7–S8, see Supporting Information). We observe fluorescence quenching of the EY and an increase in the lifetime for the {Mo$_{132}$}@Si$_6$@EY@TBA conjugate (Table 1). With the LUMO positions of EY and {Mo$_{132}$} being at 3.05 eV and 4.19 eV, respectively [2], quenching of EY's excited state can occur through an intermolecular electron transfer from the dye to POM. Aside from fluorescence quenching, the increase in the lifetime of the EY's excited state is a result of a diminished contribution from the non-radiative pathways to the fluorescence kinetics of the EY grafted onto the POM's surface.

Table 1. Absolute quantum yield and lifetime of the excited state for EY and {Mo$_{132}$}@Si$_6$@EY@TBA in different organic solvents.

	EY		**{Mo$_{132}$}@Si$_6$@EY@TBA**	
Solvent	Φ_F, %	τ, ns	Φ_F, %	τ, ns
DCM *	7.3	3.58	2.5	4.27
CHCl$_3$ *	4.7	3.3	2.4	3.91
THF	68.8	3.88	2.6	4.42
MeCN	77.6	4	2.6	4.47
Acetone	-	4.29	2.6	4.52
MeOH	54.9	2.95	1.3	3.16

Notation: * EY is slightly soluble in these solvents; Φ_F is absolute quantum yield; and τ is lifetime of excited state.

Potential reasons to observe these lifetime values for the {Mo$_{132}$}@Si$_6$@EY@TBA conjugate are as follows: (i) a decrease in the vibrational relaxation rate due to the restricted molecular motion of the EY molecule within the TBA shell on the POM's surface; (ii) reabsorption of the emitted light into the charge-transfer band. The latter would be an example of the "ping-pong" mechanism of the PET process in the {Mo$_{132}$}@Si$_6$@EY@TBA conjugate, which can be utilized for photocatalytic applications.

3. Experimental Section

3.1. Materials and Methods

3-aminopropyltrimethoxysilane (APTMS) and tetrabutylammonium bromide (TBABr) were purchased from Sigma-Aldrich. All reagents were analytical-grade and used without further purification.

The IR spectra were collected in the ATR mode on a Nicolet 6700 FT-IR spectrometer (Thermo Scientific). The obtained IR spectra were corrected in the OMNIC software to level the dependency of the IR absorbance on the wavelength. The Raman spectra were measured on an Alpha 300 AR confocal Raman microscope (WiTec GmbH). The laser (633 nm and 488 nm) beam power was set to a low value to prevent the destruction of the POM within the samples. Steady-state fluorescence measurements, absolute quantum yield, and time-resolved fluorescence decay measurements were performed with FS5 Spectrofluorometer (Edinburgh Instruments) equipped with an SC-30 integration sphere and with a nanosecond light-emitting diode (LED) (292.8 nm) using time-correlated single-photon counting. For time-resolved spectroscopy, the optical density of the sample was not higher than 0.1. The UV-Vis spectra were collected at 25 °C on a Solar-Lab PB2201 spectrometer equipped with a temperature-controlled cuvette holder. ^{1}H NMR spectra were measured using the NMR spectrometer Avance (Bruker) with a working frequency of 500 MHz. The elemental analysis (Mo, Si) was performed with an iCAP 6300 Duo atomic emission spectrometer (Thermo Scientific). The CNH analysis was performed using a CHNS Euro EA 3000 analyzer (Eurovector Instruments).

3.2. Synthesis of {Mo$_{132}$}@Si$_6$@504TBA

The {Mo$_{132}$} was prepared through a standard protocol [39], and the Keplerate structure was characterized with IR and Raman spectroscopy and then compared to the literature [30].

The modification of Keplerate by APTMS molecules was performed in accordance with a published procedure [28]. Briefly, 0.19 g of {Mo$_{132}$} (6.64 mmol) was added to the 50 mL of freshly distilled methanol and mixed vigorously under argon flow for 10 min in a 100 mL round-bottom flask. While POM was dissolving, 29.65 μL of APTMS was added to 5 mL of methanol to obtain a stock solution (stock 1). A total of 1000 μL of stock 1 (39.14 mmol of APTMS) was transferred into a syringe filled with argon and added drop-wise to the {Mo$_{132}$} methanol solution. The syringe was additionally rinsed with 1 mL of methanol; then, the washing solution was added to the reaction mixture to transfer the residual amount of APTMS into the reaction vessel. The reaction mixture was kept under an argon atmosphere for 24 h. When the reaction was complete, 50 mL of toluene was added to obtain a brown-colored precipitate. The resulting suspension was vigorously stirred for 10 min, and then the precipitate was collected by centrifugation at 6000 rpm for 10 min. To purify the sample, 12 mL of toluene was added to the collected powder, and the obtained mixture was vortexed at 2700 rpm for 10 min. Then, the precipitate was separated by centrifugation (6000 rpm/10 min). This washing cycle with 12 mL of toluene was repeated one more time. After purification, the obtained product {Mo$_{132}$}@Si$_6$ was dried in the fume hood for 24 h.

The integrity of {Mo$_{132}$} was affirmed with IR and Raman spectroscopy (see "Results and discussion"). The composition of {Mo$_{132}$}@Si$_6$ was determined by elemental analysis with the Mo:Si ratio being equal to 132:6.

In order to increase the solubility of the {Mo$_{132}$}@Si$_6$ in organic solvents, 0.2 g of {Mo$_{132}$}@Si$_6$ was dissolved in water and mixed with 50 mL of chloroform with 1.1352 g of TBABr (504 molecules of TBA per one {Mo$_{132}$}). After vigorously stirring the water–chloroform mixture, the brown chloroform phase was collected using a separation funnel. The obtained organic phase was washed with water (three times) and brine solution. Then, chloroform was removed on the rotary evaporator at 40 °C under vacuum to produce the {Mo$_{132}$}@Si$_6$@504TBA powder.

3.3. Synthesis of {Mo$_{132}$}@Si$_6$@EY@TBA

3.3.1. Synthesis of EY-NHS

In a 50 mL round-bottom flask, 1.5 g of dipotassium eosin Y salt (2.07 mmol) was dissolved in 40 mL of acetonitrile. A total of 0.2431 g of NHS powder (2.11 mmol) was added to the reaction mixture and heated using a reflux setup under an argon atmosphere for 30 min. Then, 0.44 g of DCC (2.07 mmol) was dissolved in 6 mL of acetonitrile and added to the reaction mixture under an argon atmosphere. The resulting solution was slightly heated under an argon atmosphere for 2 h. After that, the solution was left to stir overnight at room temperature. When the reaction was complete, the acetonitrile solution was stored in the fridge at 4 °C for several hours. The precipitated DCU was removed by filtering the solution through a glass frit filter, followed by washing with acetone to collect any residual amounts of EY-NHS. Then, the acetonitrile–acetone mixture was evaporated under vacuum, and EY-NHS was dissolved in chloroform to purify the sample from any residual EY (poorly soluble in CHCl$_3$ as compared to EY-NHS.) Finally, chloroform was evaporated under vacuum conditions, and the EY-NHS product was collected.

The EY-NHS structure was confirmed with ^{1}H NMR spectroscopy (in CD$_3$CN). Due to the equilibrium between the open and closed (spiro) forms of EY, the dipotassium salt of EY NMR bands appear as follows: ^{1}H NMR (500 MHz, CD$_3$CN) δ 8.10 (d, J = 7.9 Hz, 1H), 8.07 (d, J = 7.4 Hz, 0.5H), 7.54 (t, J = 6.9 Hz, 1H), 7.51–7.45 (m, 2H), 7.13–7.09 (m, 3.5H), 6.75 (d, J = 9.4 Hz, 0.5H), and 6.30 (d, J = 9.4 Hz, 0.5H). For EY-NHS, only the open form can exist: ^{1}H NMR (500 MHz, CD$_3$CN) δ 8.31 (d, J = 8.0 Hz, 1H), 7.92 (tt, J = 9.0, 4.5 Hz, 1H), 7.81 (m, 1H), 7.74–7.68 (m, 0.4H), 7.66–7.60 (m, 0.8H), 7.48 (dd, J = 7.6, 4.6 Hz, 1H), 7.37–7.33 (m, 0.4H), 7.22 (s, 0.4H), 7.18 (s, 0.2H), 7.00 (s, 0.4H), 6.80 (m, 0.2H), 6.62 (m, 0.5H), 6.36–6.28 (m, 0.8H), 4.06 (q, J = 7.1 Hz, 0.6H), 3.45–3.34 (m, 0.8H), 2.68 (d, J = 2.4 Hz, 4.4H), and 1.89–1.02 (m). Based on the NMR data, we found the presence of both EY-NHS and its

association with DCU (EY-NHS@DCU). Because this molecular associate does not inhibit the reactivity of NHS-ester, the obtained EY-NHS was used without further purification.

3.3.2. Grafting of EY-NHS to the $\{Mo_{132}\}@Si_6@504TBA$

In a 50 mL round-bottom flask, 100 mg of $\{Mo_{132}\}@Si_6@504TBA$ was dissolved in 20 mL of acetonitrile. Separately, 2.6 mg of EY-NHS was dissolved in 6 mL of acetonitrile, and 3 mL of the obtained solution was added to the reaction mixture, followed by the addition of 1 drop (~1.0 μL) of triethylamine (TEA). The molar ratio of $\{Mo_{132}\}@Si_6$:EY-NHS:TEA was 1:1:2. The reaction mixture was kept under an argon atmosphere for 24 h. Then, the solvent was removed on a rotary evaporator under vacuum at 40 °C. The obtained powder product was dissolved in 5 mL of chloroform and transferred to a glass vial. To wash the product from unhydrolyzed EY-NHS and free EY molecules, 5 mL of water was added. The mixture was vigorously stirred, and after a phase separation occurred, the concentration of EY in water was determined with UV-Vis spectroscopy. The described washing cycle was repeated four times until the aqueous phase became colorless. After the washing procedure, the chloroform was removed on a rotary evaporator under vacuum, and the $\{Mo_{132}\}@Si_6@EY@TBA$ product was collected in a solid form.

4. Conclusions

Here, we demonstrate a powerful approach for covalently grafting an organic dye —eosin Y—to the Keplerate POM $\{Mo_{132}\}$ through an APTMS linker in a series of different organic solvents: acetonitrile, acetone, THF, and DCM. The high reactivity of APTMS and its exclusive affinity with the $\{Mo_2\}$ units allowed us to perform target modifications of $\{Mo_{132}\}$ with precise stoichiometric control and functionalize POM with six $\{Si(CH_2)_3NH_2\}$ groups. The obtained $\{Mo_{132}\}@Si_6$ cluster was transferred to chloroform with a 504-fold molar excess of TBAB and then used to further react with EY-NHS ester in different aprotic organic solvents to achieve the desired dye-POM conjugate. For the resulting $\{Mo_{132}\}@Si_6@EY@TBA$ conjugate, the integrity of the Keplerate structure, as well as the absence of any NHS-ester traces within the sample, was affirmed with IR and Raman spectroscopy. ^{1}H NMR data showed significant deshielding of the dye's phenyl proton signals and pointed to the change in the open-closed form's ratio of EY from 2:1 to 1:1 upon the dye's grafting to the POM's structure. The UV-Vis spectra showed a novel charge-transfer band (from POM to the dye) for the $\{Mo_{132}\}@Si_6@EY@TBA$ conjugate in a series of organic solvents. Steady-state and time-resolved fluorescence measurements pointed to the fluorescence quenching of EY and an increase in the lifetime of its excited state upon the dye's grafting to one of the $\{Mo_{132}\}@Si_6$ units. The roles of the EY's open-closed form equilibrium and the "ping-pong" mechanism of the PET process between POM and dye were discussed. Finally, this synthetic approach can be readily applied to grafting dye and other organic molecules bearing carboxyl groups to the giant POM structure—particularly, to $\{Mo_{132}\}$—to design new supramolecular photocatalytic ensembles.

References

1. Grzhegorzhevskii, K.; Ostroushko, A.; Koriakova, O.; Ovchinnikova, I.; Kim, G. Photoinduced Charge Transfer in the Supramolecular Structure Based on Toroid Polyoxomolibdate Mo138 and Xanthene Dye—Rhodamine-B. *Inorg. Chim. Acta* **2015**, *436*, 205–213. [CrossRef]
2. Fazylova, V.; Shevtsev, N.; Mikhailov, S.; Kim, G.; Ostroushko, A.; Grzhegorzhevskii, K. Fundamental Aspects of Xanthene Dye Aggregation on the Surfaces of Nanocluster Polyoxometalates: H- to J-Aggregate Switching. *Chem. A Eur. J.* **2020**, *26*, 5685–5693. [CrossRef] [PubMed]
3. Grzhegorzhevskii, K.; Haouas, M.; Lion, M.; Vashurin, A.; Denikaev, A.; Marfin, Y.; Kim, G.; Falaise, C.; Cadot, E. Gigantic Supramolecular Assemblies Built from Dynamic Hierarchical Organization between Inorganic Nanospheres and Porphyrins. *Chem. Commun.* **2023**, *59*, 86–89. [CrossRef] [PubMed]
4. Lamare, R.; Ruppert, R.; Boudon, C.; Ruhlmann, L.; Weiss, J. Porphyrins and Polyoxometalate Scaffolds. *Chem. A Eur. J.* **2021**, *27*, 16071–16081. [CrossRef]
5. Ahmed, I.; Farha, R.; Goldmann, M.; Ruhlmann, L. A Molecular Photovoltaic System Based on Dawson Type Polyoxometalate and Porphyrin Formed by Layer-by-Layer Self Assembly. *Chem. Commun.* **2013**, *49*, 496–498. [CrossRef] [PubMed]
6. Black, F.A.; Jacquart, A.; Toupalas, G.; Alves, S.; Proust, A.; Clark, I.P.; Gibson, E.A.; Izzet, G. Rapid Photoinduced Charge Injection into Covalent Polyoxometalate–Bodipy Conjugates. *Chem. Sci.* **2018**, *9*, 5578–5584. [CrossRef]
7. Luo, Y.; Maloul, S.; Wächtler, M.; Winter, A.; Schubert, U.S.; Streb, C.; Dietzek, B. Is Electron Ping-Pong Limiting the Catalytic Hydrogen Evolution Activity in Covalent Photosensitizer–Polyoxometalate Dyads? *Chem. Commun.* **2020**, *56*, 10485–10488. [CrossRef] [PubMed]
8. Luo, Y.; Maloul, S.; Endres, P.; Schönweiz, S.; Ritchie, C.; Wächtler, M.; Winter, A.; Schubert, U.S.; Streb, C.; Dietzek, B. Organic Linkage Controls the Photophysical Properties of Covalent Photosensitizer–Polyoxometalate Hydrogen Evolution Dyads. *Sustain. Energy Fuels* **2020**, *4*, 4688–4693. [CrossRef]
9. Toupalas, G.; Karlsson, J.; Black, F.A.; Masip-Sánchez, A.; López, X.; Ben M'Barek, Y.; Blanchard, S.; Proust, A.; Alves, S.; Chabera, P.; et al. Tuning Photoinduced Electron Transfer in POM-Bodipy Hybrids by Controlling the Environment: Experiment and Theory. *Angew. Chem. Int. Ed.* **2021**, *60*, 6518–6525. [CrossRef] [PubMed]
10. Ben M'Barek, Y.; Rosser, T.; Sum, J.; Blanchard, S.; Volatron, F.; Izzet, G.; Salles, R.; Fize, J.; Koepf, M.; Chavarot-Kerlidou, M.; et al. Dye-Sensitized Photocathodes: Boosting Photoelectrochemical Performances with Polyoxometalate Electron Transfer Mediators. *ACS Appl. Energy Mater.* **2020**, *3*, 163–169. [CrossRef]
11. Huo, Z.; Liang, Y.; Yang, S.; Zang, D.; Farha, R.; Goldmann, M.; Xu, H.; Antoine, B.; Matricardi, E.; Izzet, G.; et al. Photocurrent Generation from Visible Light Irradiation of Covalent Polyoxometalate–Porphyrin Copolymers. *Electrochim. Acta* **2021**, *368*, 137635. [CrossRef]
12. Saad, A.; Oms, O.; Dolbecq, A.; Menet, C.; Dessapt, R.; Serier-Brault, H.; Allard, E.; Baczko, K.; Mialane, P. A High Fatigue Resistant, Photoswitchable Fluorescent Spiropyran–Polyoxometalate–BODIPY Single-Molecule. *Chem. Commun.* **2015**, *51*, 16088–16091. [CrossRef] [PubMed]
13. Parrot, A.; Bernard, A.; Jacquart, A.; Serapian, S.A.; Bo, C.; Derat, E.; Oms, O.; Dolbecq, A.; Proust, A.; Métivier, R.; et al. Photochromism and Dual-Color Fluorescence in a Polyoxometalate-Benzospiropyran Molecular Switch. *Angew. Chem. Int. Ed.* **2017**, *56*, 4872–4876. [CrossRef] [PubMed]
14. Zhang, J.; Huang, Y.; Li, G.; Wei, Y. Recent Advances in Alkoxylation Chemistry of Polyoxometalates: From Synthetic Strategies, Structural Overviews to Functional Applications. *Coord. Chem. Rev.* **2019**, *378*, 395–414. [CrossRef]
15. Anyushin, A.V.; Kondinski, A.; Parac-Vogt, T.N. Hybrid Polyoxometalates as Post-Functionalization Platforms: From Fundamentals to Emerging Applications. *Chem. Soc. Rev.* **2020**, *49*, 382–432. [CrossRef] [PubMed]

16. Xia, Z.; Lin, C.; Yang, Y.; Wang, Y.; Wu, Z.; Song, Y.; Russell, T.P.; Shi, S. Polyoxometalate-Surfactant Assemblies: Responsiveness to Orthogonal Stimuli. *Angew. Chem. Int. Ed.* **2022**, *61*, e202203741. [CrossRef]

17. Joo, N.; Renaudineau, S.; Delapierre, G.; Bidan, G.; Chamoreau, L.-M.; Thouvenot, R.; Gouzerh, P.; Proust, A. Organosilyl-/Germyl Polyoxotungstate Hybrids for Covalent Grafting onto Silicon Surfaces: Towards Molecular Memories. *Chem. A Eur. J.* **2010**, *16*, 5043–5051. [CrossRef]

18. Liu, T.; Diemann, E.; Li, H.; Dress, A.W.M.; Müller, A. Self-Assembly in Aqueous Solution of Wheel-Shaped Mo_{154} Oxide Clusters into Vesicles. *Nature* **2003**, *426*, 59–62. [CrossRef]

19. Zhang, J.; Li, D.; Liu, G.; Glover, K.J.; Liu, T. Lag Periods during the Self-Assembly of {$Mo_{72}Fe_{30}$} Macroions: Connection to the Virus Capsid Formation Process. *J. Am. Chem. Soc.* **2009**, *131*, 15152–15159. [CrossRef]

20. Fan, D.; Hao, J. Phase Stability of Keplerate-Type Polyoxomolybdates Controlled by Added Cationic Surfactant. *J. Colloid Interface Sci.* **2009**, *333*, 757–763. [CrossRef]

21. Liu, T.; Imber, B.; Diemann, E.; Liu, G.; Cokleski, K.; Li, H.; Chen, Z.; Müller, A. Deprotonations and Charges of Well-Defined {$Mo_{72}Fe_{30}$} Nanoacids Simply Stepwise Tuned by PH Allow Control/Variation of Related Self-Assembly Processes. *J. Am. Chem. Soc.* **2006**, *128*, 15914–15920. [CrossRef] [PubMed]

22. Kistler, M.L.; Bhatt, A.; Liu, G.; Casa, D.; Liu, T. A Complete Macroion−"Blackberry" Assembly−Macroion Transition with Continuously Adjustable Assembly Sizes in {Mo_{132}} Water/Acetone Systems. *J. Am. Chem. Soc.* **2007**, *129*, 6453–6460. [CrossRef] [PubMed]

23. Kistler, M.L.; Patel, K.G.; Liu, T. Accurately Tuning the Charge on Giant Polyoxometalate Type Keplerates through Stoichiometric Interaction with Cationic Surfactants. *Langmuir* **2009**, *25*, 7328–7334. [CrossRef] [PubMed]

24. Cameron, J.M.; Guillemot, G.; Galambos, T.; Amin, S.S.; Hampson, E.; Mall Haidaraly, K.; Newton, G.N.; Izzet, G. Supramolecular Assemblies of Organo-Functionalised Hybrid Polyoxometalates: From Functional Building Blocks to Hierarchical Nanomaterials. *Chem. Soc. Rev.* **2022**, *51*, 293–328. [CrossRef] [PubMed]

25. Izzet, G.; Abécassis, B.; Brouri, D.; Piot, M.; Matt, B.; Serapian, S.A.; Bo, C.; Proust, A. Hierarchical Self-Assembly of Polyoxometalate-Based Hybrids Driven by Metal Coordination and Electrostatic Interactions: From Discrete Supramolecular Species to Dense Monodisperse Nanoparticles. *J. Am. Chem. Soc.* **2016**, *138*, 5093–5099. [CrossRef]

26. Di, A.; Schmitt, J.; da Silva, M.A.; Hossain, K.M.Z.; Mahmoudi, N.; Errington, R.J.; Edler, K.J. Self-Assembly of Amphiphilic Polyoxometalates for the Preparation of Mesoporous Polyoxometalate-Titania Catalysts. *Nanoscale* **2020**, *12*, 22245–22257. [CrossRef]

27. Grzhegorzhevskii, K.V.; Shevtsev, N.S.; Abushaeva, A.R.; Chezganov, D.S.; Ostroushko, A.A. Prerequisites and Prospects for the Development of Novel Systems Based on the Keplerate Type Polyoxomolybdates for the Controlled Release of Drugs and Fluorescent Molecules. *Russ. Chem. Bull.* **2020**, *69*, 804–814. [CrossRef]

28. Grzhegorzhevskii, K.V.; Denikaev, A.D.; Morozova, M.V.; Pryakhina, V.; Khairullina, E.; Tumkin, I.; Taniya, O.; Ostroushko, A.A. The Precise Modification of a Nanoscaled Keplerate-Type Polyoxometalate with NH2-Groups: Reactive Sites, Mechanisms and Dye Conjugation. *Inorg. Chem. Front.* **2022**, *9*, 1541–1555. [CrossRef]

29. Bellamy, L.J. *The Infra-Red Spectra of Complex Molecules*; Springer: Dordrecht, The Netherlands, 1975; ISBN 978-94-011-6017-9.

30. Grzhegorzhevskii, K.V.; Zelenovskiy, P.S.; Koryakova, O.V.; Ostroushko, A.A. Thermal Destruction of Giant Polyoxometalate Nanoclusters: A Vibrational Spectroscopy Study. *Inorg. Chim. Acta* **2019**, *489*, 287–300. [CrossRef]

31. Bo, C.; Miró, P. On the Electronic Structure of Giant Polyoxometalates: Mo_{132} vs. $W_{72}Mo_{60}$. *Dalton Trans.* **2012**, *41*, 9984. [CrossRef]

32. Vosgröne, T.; Meixner, A.J. Surface- and Resonance-Enhanced Micro-Raman Spectroscopy of Xanthene Dyes: From the Ensemble to Single Molecules. *ChemPhysChem* **2005**, *6*, 154–163. [CrossRef] [PubMed]

33. Mchedlov-Petrossyan, N.O.; Kukhtik, V.I.; Bezugliy, V.D. Dissociation, Tautomerism and Electroreduction of Xanthene and Sulfonephthalein Dyes in *N*,*N*-Dimethylformamide and Other Solvents. *J. Phys. Org. Chem.* **2003**, *16*, 380–397. [CrossRef]

34. Kopilevich, S.; Gil, A.; Garcia-Ratés, M.; Bonet-Ávalos, J.; Bo, C.; Müller, A.; Weinstock, I.A. Catalysis in a Porous Molecular Capsule: Activation by Regulated Access to Sixty Metal Centers Spanning a Truncated Icosahedron. *J. Am. Chem. Soc.* **2012**, *134*, 13082–13088. [CrossRef] [PubMed]

35. Xu, S.; Wang, Y.; Zhao, Y.; Chen, W.; Wang, J.; He, L.; Su, Z.; Wang, E.; Kang, Z. Keplerate-Type Polyoxometalate/Semiconductor Composite Electrodes with Light-Enhanced Conductivity towards Highly Efficient Photoelectronic Devices. *J. Mater. Chem. A* **2016**, *4*, 14025–14032. [CrossRef]

36. Roth, H.; Romero, N.; Nicewicz, D. Experimental and Calculated Electrochemical Potentials of Common Organic Molecules for Applications to Single-Electron Redox Chemistry. *Synlett* **2015**, *27*, 714–723. [CrossRef]

37. De, S.; Das, S.; Girigoswami, A. Environmental Effects on the Aggregation of Some Xanthene Dyes Used in Lasers. *Spectrochim. Acta Part A Mol. Biomol. Spectrosc.* **2005**, *61*, 1821–1833. [CrossRef] [PubMed]

38. Lakowicz, J.R. *Principles of Fluorescence Spectroscopy*, 3rd ed.; Springer: Boston, MA, USA, 2006; ISBN 0-387-31278-1.

39. Müller, A.; Krickemeyer, E.; Bögge, H.; Schmidtmann, M.; Peters, F. Organizational Forms of Matter: An Inorganic Super Fullerene and Keplerate Based on Molybdenum Oxide. *Angew. Chemie Int. Ed.* **1998**, *37*, 3359–3363. [CrossRef]